Petroleum Science 20 (2023) 526–539

Contents lists available at ScienceDirect

Petroleum Science

journal homepage: www.keaipublishing.com/en/journals/petroleum-science

Original Paper

Wax deposition modeling in oil-water stratified pipe flow

Hui-Shu Liu [a, b], Ji-Miao Duan [b, *], Jiang Li [b], Jian Wang [b], Hao Yan [b], Ke-Yu Lin [b], Ke-Cheng Gu [b], Chang-Jun Li [a, **]

[a] Petroleum Engineering School, Southwest Petroleum University, Chengdu, 610500, China
[b] Petroleum, Oil and Lubricants Department, Army Logistics Academy, Chongqing, 401311, China

ARTICLE INFO

Article history:
Received 17 April 2022
Received in revised form
22 September 2022
Accepted 23 September 2022
Available online 30 September 2022

Edited by Xiu-Qiu Peng

Keywords:
Wax deposition
Oil-water flow
Stratified flow
Heat and mass transfer

ABSTRACT

Wax deposition in oil-water stratified flow is commonly encountered onshore and offshore oil production pipe systems, and typically reduces transportation capacity of oil. The accurate predicted model of wax deposition has becomes an indispensable approach to design effective remediation strategies. However, a reliable mechanistic model for wax deposition prediction in oil-water two-phase stratified pipe flow is lacking to validate the deposition process. In this work, a three-dimensional (axial, radial, and angular) robust wax deposit model for oil-water stratified circular pipe flow was developed. The model of formation of a gel deposit based on the first principles of rheology was developed, associated with the results obtained from hydrodynamics and heat/mass transfer simulations. The predictions for wax deposition are found to compare satisfactorily with experimental data with two different oils for single phase and four different water cuts for oil-water stratified pipe flow. It can be seen from the wax gelation mechanism that an increase in water cut can help to reduce the wall/oil-deposit interface shear stress, thereby leading to an increase in the degree of gelation as well as the deposit rate. Furthermore, a local deposit analysis in the circumferential direction was conducted, for water cut 75% and total flow rate 5 m^3/h, which provided insights to understand that the thickness on pipe wall was roughly uniformly distributed locates near the top of the pipe and the nearer the position gets close to two points, where the oil-water interface contacts the inner wall, the deposition thickness quickly dropped to 0. It was attributed to the fact that a roughly uniformly thickness far away from the oil-water interface contact the inner wall resulted in the slowly changes temperature along the circumferential pipe wall wetted by oil.

1. Introduction

With the decrease of onshore and offshore oil and gas resources, the development is performed from offshore to the deep and ultra-deep water (Bai et al., 2019). As the deep and ultra-deep water drilling becomes increasingly important in the petroleum industry, water is commonly seen in the subsea pipelines. Oil-water two-phase pipe flow occurs widely during the production and transportation of oil in the industry. There are some flow patterns, such as stratified, stratified wavy with droplets at the interface, dispersion of oil in water with water layer, dispersion of water in oil with oil layer, dual continuous, dispersion of oil in water, dispersion of water in oil, slugs of one liquid into the other, annular flow (one of the liquids forms the core and the other liquid flows in the annulus), observed along the pipe, as shown in.

Fig. 1. Wax deposition in oil-water two-phase flow requires significant attention. Affected by the low temperature environment of seabed (deep water seabed temperature is approximately 4 °C), when crude oil extracted from the reservoir flows through the submarine mixed transmission pipeline, the crude oil temperature near pipe wall will drop below wax appearance temperature (WAT), and wax molecules dissolved in the crude oil near pipe wall will crystallize out and deposit on pipe wall or formed immobile layer by its free surface energy. The occurrence of wax deposition in pipeline transportation system reduces effective circulation area of the pipeline, reduces transportation capacity of the pipeline, and even leads to wax plugging accident in serious cases (Liu et al., 2020).

* Corresponding author.
** Corresponding author.
E-mail addresses: hsliu0820@163.com (H.-S. Liu), duanjimiao@126.com (J.-M. Duan), lijiang830@163.com (J. Li), 1063426510@qq.com (J. Wang), amanscut@sina.com (H. Yan), 923763050@qq.com (K.-Y. Lin), 278508597@qq.com (K.-C. Gu), lichangjunemail@sina.com (C.-J. Li).

https://doi.org/10.1016/j.petsci.2022.09.028

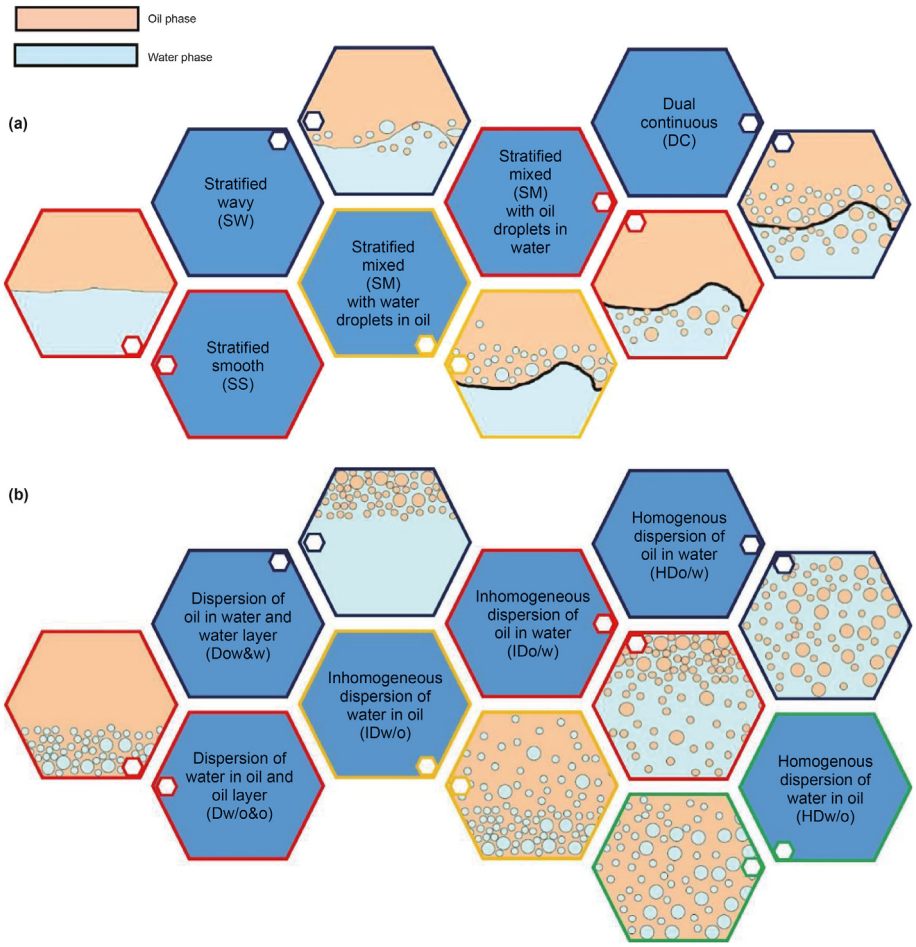

Fig. 1. Oil-water flow pattern classifications: (**a**) separated flows and (**b**) dispersed flows (Piroozian et al., 2017).

1.1. Wax deposition mechanism

So far, various mechanisms have been proposed for the wax deposition in the single phase pipe flow, including Brownian diffusion, gravity deposition, Soret diffusion, shear dispersion, shear reduction, gelation and molecular diffusion (Van der Geest et al., 2021). When the bulk temperature of oil is higher than WAT, molecular diffusion is generally considered to be the most important driving force of the wax molecules radial diffusion, and plays a leading role in the wax deposit, while the other mechanisms have little influence (Yang et al., 2020).

At present, a preliminary study has been made on the wax deposition of the bulk oil temperature below WAT, and it is found that some experimental phenomena cannot be explained by molecular diffusion mechanism (Mahir et al., 2019, 2021). Van Der Geest et al. (2018) found that when the temperature of the bulk oil approached WAT, wax deposition did not start immediately and was delayed, which could not be explained by molecular diffusion mechanism. Janamatti et al. (2019) and Yang et al. (2020) found that when the oil temperature equals to the wall temperature and below the WAT, wax deposition occurs on the pipe wall, which is in contradiction with the traditional conclusion that wax deposition can occur only when the oil temperature is higher than the wall temperature. At the same time, the wax deposition decreases with the increase of the difference temperature between oil and pipe wall, increases with the decrease of the wall temperature, and increases with the decrease of the oil flow rate, which is contrary to the traditional conclusion that the increase of the difference temperature between oil and pipe wall, which will increase the driving force of the diffusion of wax molecules and thus increase the wax deposit. Further analysis of the carbon distribution of n-alkanes in the deposit layer shows that the composition of the layer under low difference temperature between oil and pipe wall is very similar to crude oil, which indicating that the aging effect is weak and the gelation effect is obvious. Mahir (2020; 2021) found that molecular diffusion was one of the factors leading the increase of local yield stress of the deposit layer, rather than the prerequisite of wax deposit. Meanwhile, wax deposit needs to consider the gelation of crude oil, and proposed a wax deposit model of coupling transient heat transfer and transient mass transfer. The transient mass transfer describes the classic diffusion of wax molecules, and the transient heat transfer process describes the phase transition of wax precipitation on the surface of the layer, which is gelation. They point out that both mechanisms must be considered during wax deposit. However, there is a lack of further analysis on which is the leading mechanism of wax deposit under operating conditions.

1.2. Wax deposition in oil-water stratified flow

Accurate prediction of wax deposition is of great importance to develop economical prevention and remediation strategies (Zhang et al., 2022). In wax deposition modeling, knowledge of the hydrodynamics, heat transfer, and mass transfer are the major challenges in oil-water two-phase flow because there are a variety of

flow patterns and each pattern has its own unique transport phenomena (Huang et al., 2011a,b). Oil-water stratified flow will be examined in this research because it often presents in horizontal or slightly inclined systems in gravity filed, and it is considered to be among the fundamental flow configuration in two-phase systems.

Until now, only four studies (Anosike, 2007; Bordalo and Oliveira, 2007; Hoffmann et al., 2012; Quan et al., 2015) are reported on the experimental characteristics of the oil-water two-phase stratified flow wax deposition. Bordalo and Oliveira (2007) studied artificial waxy oil-water two-phase stratified wax deposition by the loop experiment. Different from the ideal stratified flow pattern, there is a water film on the upper part of the pipe wall, that is, the oil phase does not directly contact the pipe wall, but wax deposition is still observed on the pipe wall. Furthermore, wax deposition occurs only on the upper of pipe wall. They explain that although the water film prevents wax particles contacting the wall, its blocking effect is limited because it is very thin and discontinuous. Anosike (2007) investigated wax deposition under oil-water flow conditions in order to ascertain the effects of flow pattern and water fraction on deposition behavior. It observed that wax deposit does not occur at the bottom of the pipe for stratified flows. The deposit distributed only along the top half of the pipe is very soft and very similar to the corresponding single phase laminar deposit, and the thickness distribution along the circumference is uneven. Little or no water fraction was observed in the deposit. As the superficial water velocity increased, the hardness of the wax deposit increased and the thickness decreased. Hoffmann et al. (2012) carried out wax deposition experiments in oil-water stratified flow in a 2-inch loop using the North Sea gas condensate and formation water, at various water cuts with the total flow rates of 5 and 10 m^3/s, to investigate the effect of the presence of water on wax deposition. A laser-based measurement technique is used to document the wax thickness distributed around the pipe circumference. The wax deposition occurs only on the upper of pipe wall and the wax thickness is zero at the bottom of the pipe where there is a plateau, as shown in Fig. 2, and the thickness distribution is non-uniform. The coexistence of the two mechanisms in deposit formation, which are diffusion and gelation, are proposed, through analysis the carbon number distributions of the deposit. The degree of wax gelation as well as the thickness of deposit increase with the shear stress in the oil decrease. Quan et al. (2015) performed the wax deposition experiments of emulsion-water stratified pipe flow with variable flow rate of oil-water mixture. The circumferential deposit thickness distribution is measured by the laser thickness gauge. Wax deposition builds up only on the top of the pipe connected with water-in-oil emulsion. The degree of the gelation increases as the water cut of emulsion increases. In addition, the deposit thickness increases first and then decreases, as the total water cut decreases.

The oil-water two-phase flow wax deposition is poorly understood. The wax deposition modeling studies for stratified flow are limited in the published literatures. The currently available models, such as Huang et al. (2011a,b) and Quan et al. (2015), apply the single-phase deposition model with overall multiphase hydrodynamic and heat transfer models. Huang et al. (2011a,b) developed a deposition model for stratified oil-water channel flow, not applicable for field-scale circular pipe. It is found that the presence of water significantly reduces the wax deposition thickness by altering the heat and mass transfer characteristics caused by the water phase. This is inconsistent with the experiment of Hoffmann et al. (2012). Quan et al. (2015) proposed the emulsion-water stratified wax deposit model applying the molecule diffusion and gelation. However, they didn't give the reason why the deposition thickness distribution is roughly uniform.

There is no wax deposit model available strictly for oil-water stratified two-phase pipe flow, with a necessary concern of multiphase flow characteristics. In this research, a three-dimensional (axial, radial, and angular) robust wax deposit model for oil-water stratified circular pipe flow is developed. The model of formation of a gel deposit based on the first principles of rheology is developed, associated with the results obtained from multiphase transfer simulations. The effect of stratified flow pattern on the two-phase oil-water wax deposition, how water influences on deposit, and the deposit circumferential distribution are investigated.

2. Wax deposition model

Wax deposition is mainly a heat and mass transfer driven phenomenon. In wax deposition modeling, knowledge of the hydrodynamics and heat/mass transfer are the major challenges in two-phase flow. The wax deposition model consists of four sequential calculation steps: (1) a hydrodynamic calculation, (2) a heat transfer calculation, (3) a mass transfer calculation, and (4) a deposit growth calculation (Duan et al., 2016, 2017). Non-isothermal hydrodynamics, heat and mass transport are calculated for three phases (oil, water, and deposit) in modeling wax deposition of oil-water stratified flow. The non-isothermal hydrodynamic model simulates the velocity profile and the eddy momentum diffusivity to be used in the heat and mass transfer calculations. Heat and mass transfer calculations predict the heat loss from oil and water to the surroundings and the molecular diffusion of wax, followed by simulation of deposit growth and aging. As the deposit grows on the pipe wall, the oil-water interface and oil-deposit interface are two moving boundaries that need to be updated at each time step, as shown in Fig. 3.

2.1. Hydrodynamics modeling

Pipe flow hydrodynamic need to be fundamentally studied to calculate the heat and mass transfer, further to predict wax deposition. The axial momentum equations for oil and water phases are used to calculate the pressure gradient, the water cut, and the velocity profile in the pipe cross section. The non-circular and irregular oil and water domain in pipe are conveniently modeled with using the bipolar coordinate system. The governing equation can be derived from three-dimensional momentum equations, considering an incompressible, fully developed stratified oil-water flow in a pipe. The oil and water two phases in stratified flow may appear the laminar or turbulent flow. In general, the water phase is more prone to turbulence than oil phase, under the same flow conditions. For the turbulent flow, the turbulent characteristic is described by using k-ε model. The turbulent eddy viscosity will be set as 0, $\mu_t = 0$, when water or oil phase keeps the laminar flow. Details of the hydrodynamic modeling and solving are available in our recently study (Liu et al., 2022).

2.1.1. Oil-water interface configuration

The flow geometry of oil-water stratified flow in circular pipe is very complex. The careful observations of the experiments confirm that the oil-water interface in stratified flow is usually not flat (Chakrabarti et al., 2005; Edomwonyi-Otu and Angeli, 2015; Santos et al., 2019), as shown in Fig. 4. The effect of surface tension and gravity on the interface configuration are characterized by the Eötvös number, Eo, given by

$$E_O = \frac{\Delta\rho g R^2}{2\sigma} \tag{1}$$

where $\Delta\rho$ is the density difference between two fluids, kg/m^3. R is

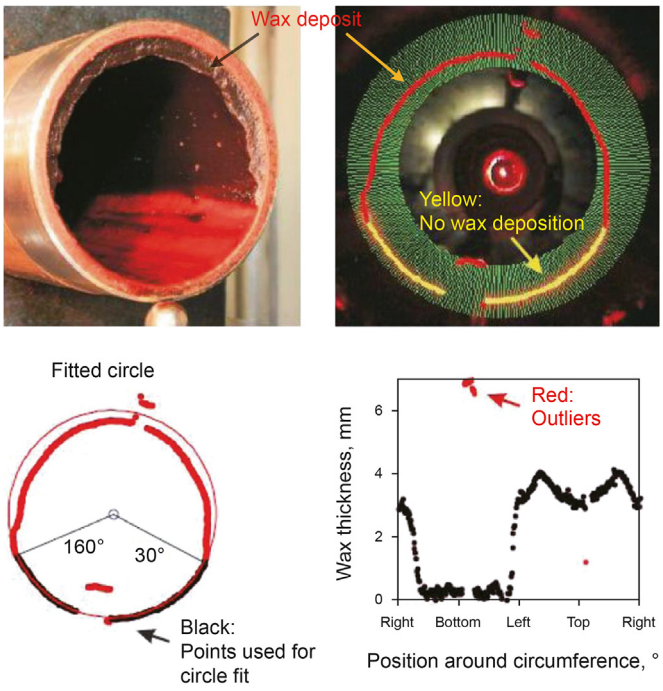

Fig. 2. Laser measurement in Hoffmann et al. (2012).

the radius of the pipe, m. σ is the interfacial tension, N/m, and g is the gravitation, m^2/s. In general, when Eötvös number E_O increases, the interface configuration tends to attain planar configuration, the smaller the E_O, the more closely the interface approaches a curve surface.

In general, it is indicated that (Liu et al., 2008) the dynamic model with planar interface assumption is applicable to the case of $E_O \geq 10$ or oil-water flow, while for the systems with E_O<10, exactly, E_O<5, this assumption causes significant deviation from actual interface geometry (Gorelik and Neima, 1999; Ng et al., 2001).

As shown in Fig. 4, TP_1 and TP_2 are the intersection points of oil-water interface and pipe wall. The arbitrary point, B, on the oil or water phase of the cross-section pipe is represented by the view angle from the angle of TP_1 and TP_2, θ. The pipe wall perimeter and the oil-water interface are iso-line. θ_0 represents the upper section of the pipe wall wetted by the oil phase. $\theta_0 + \pi$ represents the bottom of the pipe wall wetted by the water phase. θ^* represents the oil-water interface, which is a circular segment centered at O_2.

Therefore, it is convex interface for $\theta^* < \pi$, planar interface for $\theta^* = \pi$, and concave interface for $\theta^* > \pi$. θ^* is related to pipe geometry, densities and interfacial tension forces of the fluids, and solid-fluids wettability angle α. Therefore, the correlation, $\theta^* = \theta^*(\theta_0, E_O, \tilde{\alpha})$ needs a special consideration and solved by the hydrodynamic problem.

Brauner et al. (1996) assumed that the correlation, $\theta^* = \theta^*(\theta_0, E_O, \tilde{\alpha})$ corresponds to minimum the sum of the system potential energy, E_P and surface energy E_S. The total energy E is sum of the potential energy and surface energy, *i.e.*, $E = E_P + E_S$. The total energy variation for a unit length of a pipe is given by:

$$\begin{aligned}\frac{\Delta\tilde{E}}{L} &= \frac{1}{R^3 g(\rho_W - \rho_O)L}(\Delta E_P + \Delta E_S) \\ &= \left(\frac{\sin^3\theta_0}{\sin^2\theta^*}(\arctan\theta^* - \arctan\theta_0)\left(\pi - \theta^* + \frac{1}{2}\sin(2\theta^*)\right)\right. \\ &\left. + \frac{2}{3}\sin^3\theta_0^P\right) + \frac{1}{E_O}\left(\sin\theta_0\frac{\pi-\theta^*}{\sin\theta^*} - \sin\theta_0^P + \cos\alpha\left(\theta_0^P - \theta_0\right)\right)\end{aligned} \tag{2}$$

where L is the length of pipe. ρ_W and ρ_O are the density of the water and oil fluid, respectively. θ_0^P is the oil distribution angle for plane interface configuration, *i.e.*, $\theta_0^P = \theta_0(\theta^* = \pi)$. The steady oil-water interface configuration, *i.e.*, the relationship between θ^* and θ_0, can be determined by minimizing the total system energy $\Delta E/L$ in Eq. (2).

As shown in Fig. 5, the bipolar coordinate system is utilized for the circular geometry under consideration. It gives a big advantage to use finite difference method to solve the hydrodynamic equation. The intersection points of oil-water interface and pipe wall, TP_1 and TP_2, are the two polar points in bipolar coordinate system, which are set respectively as $(-a, 0)$ and $(a, 0)$ in rectangular coordinate system. a represents the half distance between the two polar points, m. η and ξ are the two axes of bipolar coordinate system, dimensionless, rad.

Bipolar coordinate system is a orthogonal coordinate system. The differential operator of the transformation between Cartesian coordinate (x, y, z) and bipolar coordinate (x, ξ, η) is to plug the scaling factor into the general equation of the orthogonal coordinate system. The scale factors of bipolar coordinate system are given as follows:

$$l_x = 1 \tag{3}$$

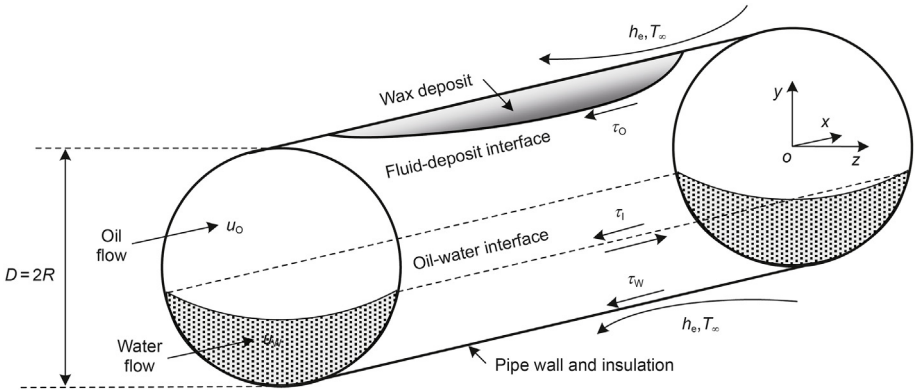

Fig. 3. Schematic representation of wax deposit in stratified oil-water flow.

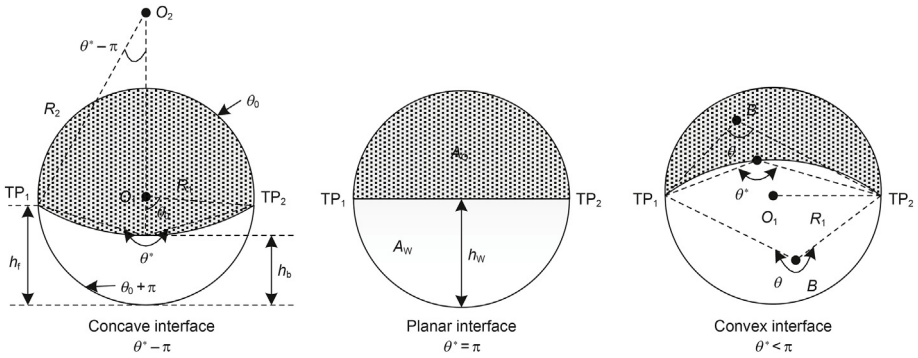

Fig. 4. Schematic of the interface geometry (Liu et al., 2022).

$$l_\xi = l_\eta = \frac{a}{\cosh\eta - \cos\xi} \tag{4}$$

Oil phase calculation domain:

$$\theta_0 < \xi < \theta^*, -\infty < \eta < +\infty \tag{5}$$

Water phase calculation domain:

$$\theta^* < \xi < \theta_0 + \pi, -\infty < \eta < +\infty \tag{6}$$

It is necessary to have a finite limit on the maximum value of η, i.e., η_{max}, in order to performance the numerical simulation. $\eta_{max} = 7$ is used in the study (Duan et al., 2017).

2.1.2. Mass conservation equation

Because of the oil and water phases immiscible, the oil and water phase mass flows remain constant at any cross section of the pipeline in the flowing direction, x. The mass conservation equation can be expressed as follows.

$$G_{in,W} = \int_{A_W} \rho_W u_W dA \tag{7}$$

$$G_{in,O} = \int_{A_O} \rho_O u_O dA \tag{8}$$

where $G_{in,O}$ and $G_{in,W}$ is the mass flow rate of oil and water at the pipe inlet respectively, kg/s. ρ_O and ρ_W is the density of oil and water respectively, kg/m^3. w_O and w_W is the axial velocity of the oil and water phase respectively, m/s. A_O and A_W is the flow area of oil and water at cross section respectively, m^2.

2.1.3. Momentum equation

The momentum equation, turbulent kinetic energy k and dissipation ε of for oil and water phase in the bipolar coordinate system can be described by the identical control equation, given as

$$\frac{1}{l_\eta l_\xi}\frac{\partial}{\partial\xi}\left(\Gamma_\varphi\frac{\partial\varphi}{\partial\xi}\right) + \frac{1}{l_\eta l_\xi}\frac{\partial}{\partial\eta}\left(\Gamma_\varphi\frac{\partial\varphi}{\partial\eta}\right) = u\frac{\partial\varphi}{\partial x} + S_\varphi \tag{9}$$

where φ is the general variable. Γ_φ and S_φ are the generalized diffusion coefficient and source term, respectively. The detail of the control equations is seen in Table 1. The identical form provides convenience for a general calculation program.

A finite difference scheme is used to discretize the governing Eq. (9) in oil and water two phases. The numerical solution of governing equations is conducted separately for each phase, with the boundary condition using an iterative finite difference technique.

2.1.4. Boundary conditions

The final elements of the model are the boundary conditions at the pipe wall, oil-water interface and vertical center line must be defined. The appropriate boundary conditions are employed according to Table 2.

2.2. Heat transfer modeling

The temperature profile is calculated using the energy balance, Eq. (10), assuming a quasi-steady state in which axial conduction is neglected.

$$\frac{1}{l_\eta l_\xi}\frac{\partial}{\partial\xi}\left(\Gamma_T\left(\frac{l_\eta}{l_\xi}\frac{\partial T}{\partial\xi}\right)\right) + \frac{1}{l_\eta l_\xi}\frac{\partial}{\partial\eta}\left(\Gamma_T\left(\frac{l_\xi}{l_\eta}\frac{\partial T}{\partial\eta}\right)\right) = w\frac{\partial T}{\partial z} \tag{10}$$

where Γ_T is the effective thermal diffusivity coefficient which is defined as the sum of the molecular thermal diffusion μ_m/Pr and eddy diffusion of heat transfer μ_t/Pr_T, $\Gamma_T = \mu_m/\mathrm{Pr} + \mu_t/\mathrm{Pr}_T$. Pr is the Prandtl number. $\mathrm{Pr} = C_P\rho\mu_m/\lambda$; C_P represents the specific heat at constant pressure of water or oil phase, J/(kg·K); λ represents

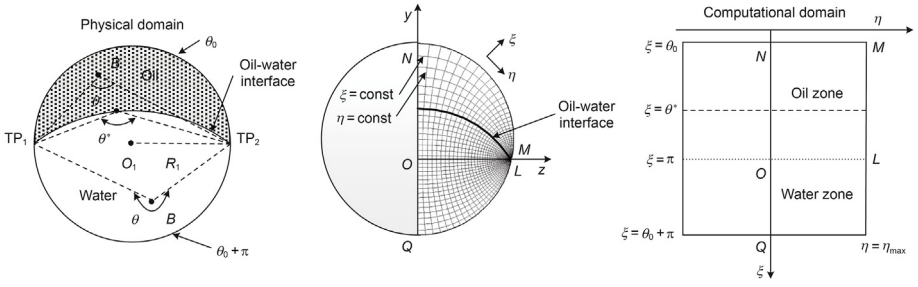

Fig. 5. Bipolar coordinate system.

the heat conductivity coefficient of water or oil, W/ (m·K). Pr_T is the turbulent Prandtl number, which is calculated by Kays method (KaysWilliam, 1994).

The thermal boundary condition assumes a constant inlet temperature and a continuous heat fluxes at the walls.

$$\begin{cases} T = T_b \text{ at } x = 0 \\ \partial T/\partial\eta = 0 \text{ at } \eta = 0 \\ T_{int,W} = T_{int,O} \text{ at } \xi = \theta* \\ -\lambda_W(\partial T/\partial\xi) = l_\xi h_e(T_{envir} - T_{wall}) \text{at } \xi = \theta_0 + \pi \\ -\lambda_{dep}(\partial T/\partial\xi) = l_\xi h_e(T_{wall} - _{envir}) \text{at } \xi = \xi_i \end{cases} \tag{11}$$

The thermal boundary condition assumes a heat flux at the walls with overall heat transfer coefficient, h_e, accounting for the thermal resistance of the wax deposit layer, the pipe wall, and the coolant.

$$\frac{1}{h_e l_{\xi_i}\xi_i} = \frac{1}{\lambda_{dep}}\ln\frac{l_{\pi+\theta_0}(\pi+\theta_0)}{l_{\xi_i}\xi_i} + \frac{1}{\lambda_{pipe}}\ln\frac{D_{in,out}}{D_{in,in}} + \frac{1}{h_O R_{out,in}} \tag{12}$$

If no wax or a very small amount of wax layer buildup on the pipe wall, the insulation would become negligible. The thermal conductivity of the gel deposit is assumed to be a function of its wax content, as given by Singh et al.

$$\lambda_{dep} = \frac{[2\lambda_{wax} + \lambda_O + (\lambda_{wax} - \lambda_O)\overline{F}_w]}{[2\lambda_{wax} + \lambda_O - 2(\lambda_{wax} - \lambda_O)\overline{F}_w]}\lambda_O \tag{13}$$

The external convective heat transfer coefficient, h_o, can be calculated from correlations specific to submerged, buried, or unburied pipelines.

2.3. Mass transfer modeling

The concentration profile is calculated using the mass balance, Eq. (14), for mass transfer in which axial diffusion is neglected. The precipitation of wax molecules in the bulk oil is neglected, which is valid for laminar flow. The mass transfer equation of wax molecules has been shown as Eq. (14).

$$\frac{1}{l_\eta l_\xi}\frac{\partial}{\partial\xi}\left(\Gamma_C\frac{l_\eta}{l_\xi}\frac{\partial C}{\partial\xi}\right) + \frac{1}{l_\eta l_\xi}\frac{\partial}{\partial\eta}\left(\Gamma_C\frac{l_\xi}{l_\eta}\frac{\partial C}{\partial\eta}\right) = w\frac{\partial C}{\partial z} \tag{14}$$

where C is the wax concentration in crude oil, kg/m^3; Γ_C is the turbulent effective wax molecule diffusivity coefficient, $\Gamma_C = \mu_m/\mathrm{Sc} + \mu_t/\sigma_C$, m^2/s; σ_C is the heat transfer diffusion coefficient resulted by turbulence; Sc represents the Schmidt number, $\mathrm{Sc} = \mu_m/D_{WO}$; D_{WO} represents the wax diffusion coefficient in crude oil, m^2/s.

The boundary conditions of mass transfer equation are described in Eq. (15). According to Eq. (15), it is assumed that the distribution of wax concentration remains constant at the cross section of pipeline inlet, $C = C_b$; the wax concentration is the saturated concentration of wax molecules in crude oil due to the assumption of wax molecules keeping solid-liquid equilibrium.

Table 1
Control equations of momentum transfer.

φ	Γ_φ	S_φ
u	$\mu_m + \mu_t$	$\frac{dP}{dx}$
k	$\mu_m + \frac{\mu_t}{\sigma_k}$	$\rho\varepsilon - \mu_t\left[\left(\frac{\partial u}{\partial\eta}\right)^2 + \left(\frac{\partial u}{\partial\xi}\right)^2\right]$
ε	$\mu_m + \frac{\mu_t}{\sigma_\varepsilon}$	$c_2 f_2 \rho\frac{\varepsilon^2}{k} - c_1 f_1 \mu_t\frac{\varepsilon}{k}\left[\left(\frac{\partial u}{\partial\eta}\right)^2 + \left(\frac{\partial u}{\partial\xi}\right)^2\right]$

Table 2
Boundary conditions of hydrodynamic calculation.

Variable	Pipe Wall	Oil-water Interface	Vertical Center Line
u	$u_W = 0$	$u_{I,O} = w_{I,W}$	$\frac{\partial u}{\partial\eta} = 0$
k	$k_W = 0$	$k_{I,O} = k_{I,W} = 0$	$\frac{\partial k}{\partial\eta} = 0$
ε	$\left.\frac{\partial\varepsilon}{\partial\eta}\right\|_W = 0$	$\left.\frac{\partial\varepsilon}{\partial\xi}\right\|_I = 0$	$\frac{\partial\varepsilon}{\partial\eta} = 0$
μ_t	$\mu_{t,W} = 0$	$(\mu_t)_{I,O} = (\mu_t)_{I,W} = 0$	–
τ	$\tau_W = \mu_m\frac{1}{l_\eta}\frac{\partial w}{\partial\eta}$	$\tau_{I,O} = \tau_{I,W}$	–

$$\begin{cases} C = C_b, z = 0 \\ \dfrac{\partial C}{\partial\eta} = 0, \eta = 0 \\ C = C_{ws}(T), \xi_i \le \xi \le \pi + \gamma \\ C = 0, \gamma \le \xi < \pi \\ \dfrac{\partial C}{\partial\xi} = 0, \xi = \pi \end{cases} \tag{15}$$

2.4. Deposition mechanism

The molecular diffusion mechanism has been widely believed to be the dominant process in wax deposition. It is often solely used to predict the deposit thickness growth and the wax content of the deposit increasing. Wax deposition formation of incipient gel layer on the wall of which the temperature is below the WAT. The gelation will form only when about 2% wax crystals precipitate from the crude oil, so there is much trapped oil in the incipient gel layer (oil trapped in a 3-D network structure of the wax crystals). Because of the low wall temperature, the molecules in gel layer or incipient deposition layer precipitate out from the crude oil, which leads to a concentration gradient of wax molecules on the fluid-deposit interface. The convective diffusion of wax molecules dissolved in oil transfer to the deposit-fluid interface precipitate and leading to deposit growth. The rest of the wax molecules continue to diffuse into the gel through the trapped oil, which enlarge the wax content in deposition layer. Zheng et al. (2017) and Huang et al. (2011a,b) points out the models solely on the basis of the molecular diffusion mechanism fail to predict the deposit growth rate and solid fraction in layer at high and low oil flow rates. Zheng et al. (2017) developed a rigorous model to predict the wax deposit thickness and the solid fraction of the depositing layer on the basis of first principles of rheology, coupling molecular diffusion mechanism and gelation mechanism, as shown in Fig. 6. The gelation can occur and form a deposit when the dynamic yield stress of the layer reaches and exceeds the shear stress imposed by the oil fluid at the pipe wall. The dynamic yield stress is positively correlated with the solid volume fraction of deposit layer. It gives good agreement with field observations for lower oil velocity, result in higher deposit thicknesses and low wax content in the deposit, which is consistent with the finding in the wax deposition experiment in stratified oil-water flow carried out by Hoffmann et al. (2012). So the wax deposit model developed by Zheng et al. (2017) is used here.

It is noted that this wax deposit model in oil-water stratified flow is 3-Dimensional. There are two items of wax mass flux at pipe cross section, i.e., the mass flux from the bulk oil to the oil-deposit interface in the direction of ξ and η in bipolar coordinate, $J_{A,\xi}$ and $J_{A,\eta}$. This is because the wax concentration C is a function of both ξ

and η, and the dissolved wax concentration gradients in the direction of ξ and η all cause wax mass flux, further contribute to wax deposit growth. It is more complex than the single phase wax deposit and the circumferential deposit thickness distribution in oil-water stratified flow is non-uniform observed by the experiment.

The thickness growth rate $d\delta_\xi/dt$ is acquired from the difference value between the convection diffusion mass flux from the pipeline center to the oil-deposit interface in the direction of ξ, $J_{A,\xi}$ and the diffusion mass flux into wax deposition $J_{B,\xi}$, as shown in Eq. (16).

$$\rho_{dep}\overline{F}(t)\frac{d\delta_\xi}{dt}=J_{wax,\xi}=J_{A,\xi}-J_{B,\xi} \tag{16}$$

Meanwhile the difference between $J_{A,\eta}$ and $J_{B,\eta}$ represents the growth of the deposit thickness in the direction of η, $d\delta_\eta/dt$ given as

$$\rho_{dep}\overline{F}(t)\frac{d\delta_\eta}{dt}=J_{wax,\eta}=J_{A,\eta}-J_{B,\eta} \tag{17}$$

In wax deposition, the wax molecules diffuse into the deposition through trapped oil, the transfer medium for wax molecules, and the wax content increases with time resulted by wax diffusion mass flux $J_{B,\xi}$ and $J_{B,\eta}$. According to the law of mass conservation, the wax content growth rate $d\overline{F}/dt$ in deposition can be obtained by Eq. (18).

$$\rho_{dep}\frac{d\overline{F}}{dt}=\left(\frac{J_{B,\xi}}{\delta_\xi}+\frac{J_{B,\eta}}{\delta_\eta}\right) \tag{18}$$

The diffusion mass flux from the bulk oil to the oil-deposit interface in the direction of ξ and η, $J_{A,\xi}$ and $J_{A,\eta}$, which can be calculated based on the concentration gradient of wax molecules, given as Eqs. (19) and (20).

$$J_{A,\xi}=-D_{wo}\frac{1}{l_\xi}\frac{dC}{d\xi}\bigg|_{\text{oil to interface}} \tag{19}$$

$$J_{A,\eta}=-\left(-D_{wo}\frac{1}{l_\eta}\frac{dC}{d\eta}\bigg|_{\text{from oil to interface}}\right) \tag{20}$$

Similarly, the diffusive mass flux from oil-deposit interface into the deposit in the direction of ξ and η, $J_{B,\xi}$ and $J_{B,\eta}$, given by Eqs. (21) and (22).

$$J_{B,\xi}=-D_{eff}\frac{1}{l_\xi}\frac{dC}{d\xi}\bigg|_{\text{from interface into deposit}} \tag{21}$$

$$J_{B,\eta}=-D_{eff}\frac{1}{l_\eta}\frac{dC}{d\eta}\bigg|_{\text{from interface into deposit}} \tag{22}$$

where D_{wo} represents the wax diffusion coefficient in crude oil. D_{wo}, depending on the oil temperature, viscosity of crude oil and molar volume of wax molecules, is calculated by Hayduk-Minhas correlation (Hayduk W, 1982). D_{eff} is the effective diffusivity of wax in the deposit calculated by the correlation of Cussler EL (1988).

$$D_{wo}=13.3\times10^{-12}\times\frac{T^{1.47}\mu^{\gamma}}{V_A^{0.71}} \tag{23}$$

$$D_{eff}=\frac{D_{wo}}{1+\alpha^2\overline{F}^2/(1-\overline{F})} \tag{24}$$

where T is the oil temperature, K; μ is the dynamic viscosity of crude oil, mPa·s; V_A is the wax molecules molar volume, cm^3/mol. α is the equivalent crystal aspect ratio. Singh et al. (2000) assumed that the α varies linearly with the wax fraction given as

$$\alpha=1+k_\alpha\overline{F} \tag{25}$$

where k_α is obtained by fitting the prediction with the available experimental results. It changes with the operating conditions.

Wax deposition formation of incipient gel layer on the wall where the temperature is below WAT, and gradually develops a yield stress, τ_y. The gelation will form only the yield stress (τ_y) exceeds the shear stress (τ_s) imposed by the fluid flow. The incipient gelation contains only 2% wax crystals precipitate from the crude oil and the yield stress, τ_y, is smaller. As the wax content increases and precipitates due to wax molecular diffusion into the deposit, the yield stress increase. The relationship between the yield stress and the solid fraction is obtained from the viscosity-temperature curves measured at different shear rates using the Herschel-Bulkley model (Chilton and Stainsby, 1998), given as

$$\mu=\frac{\tau_y+K\dot{\gamma}^n}{\dot{\gamma}} \tag{26}$$

where K is consistency of fluid, $Pa\cdot s^n$, n is flow index; $\dot{\gamma}$ is strain rate magnitude, s^{-1}.

3. Experiment

In order to test the feasibility of the wax deposition model in oil-water stratified pipe flow, the predications are compared with the experiment conducted by Hoffmann et al. (2012) with a flow loop. The single phase oil and water are injected into flow loop simultaneously using a Y-shaped mixing device, which initializes stratified flow by avoiding excessive mixing of the phases. Through a 17 m long pipe inflow section to ensure fully developed flow, the oil-water two-phase fluid flows into the 2-inch inner diameter (52.5 mm), 5.31m long test section (L_t = 5.31 m) where they are cooled by coolant and the wax deposit layer build up on the inner wall, as shown in Fig. 7. The water as a coolant circulates in an annulus surrounding the oil pipe, simulating the subsea heat transfer condition. There is 0.63m long test section (L_r = 0.63 m) can be removable. After the duration of wax deposit, the circumferential distribution of wax quantified by the laser-based technique and the weights of the deposit layer measured in the removable test section. Behind the test section, the oil-water two-phase enters the tank, to separate them into clean phases, and then they are sent back into the loop. Before the test section, the window is set for visual impression of flow regime and the X-ray tomography is set to measure the vertical water volume fraction distribution in the pipe to avoid the misleading caused by the relatively small amounts of dispersed oil in water make.

The used oil is a waxy condensate from the North Sea (Hoffmann and Amundsen, 2010). The main properties of oil are: density 809 kg/m^3 at 20 °C, WAT 30 °C, pour point 1 °C, wax content 4.5 wt %. The viscosity and the solubility curves of the oil are shown in Fig. 8, respectively. The interfacial tension of the oil-water is 11 mN/m at 20 °C. The operating conditions of the completely stratified flows experiment are shown in Table 3. The coolant temperature is set to 15 °C in all experiments. These operating conditions and

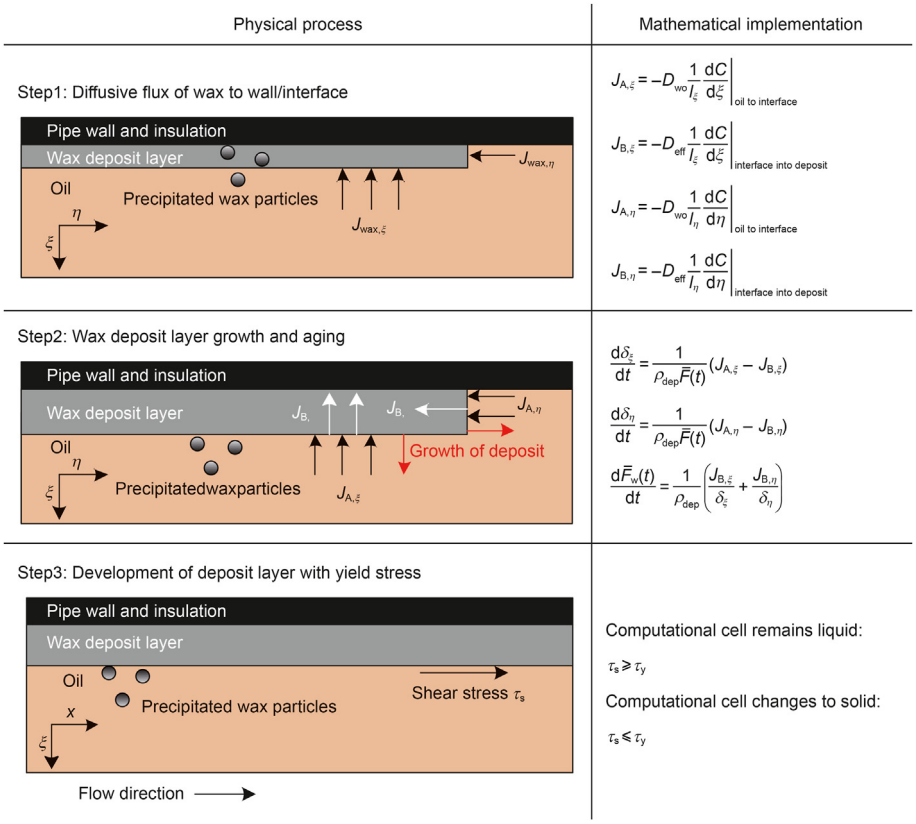

Fig. 6. Illustration of diffusion and gelation process and the mathematical implementation.

material properties are used as the inputs to the model simulation. The solubility curve of the oil is an important input parameter for wax deposition modeling. The amount of precipitation of wax in the oil at various temperatures was determined using the Differential Scanning Caborimetry (DSC), as reported by Hoffmann and Amundsen (2010). The solubility curve is obtained by assuming that all the wax has precipitated out of the oil at 6 °C. In this case, the total wax content is the same as the precipitation of wax at 6 °C. Because the coolant temperatures of all the experiments are no less than 6 °C, the wall temperatures of all the experiments are higher than 6 °C. The amount of wax precipitation in oil below the wall temperature is not needed for model predictions in this study.

In the experiment of Hoffmann et al. (2012), the completely oil-water stratified flow occurs for the water cut ranging from 30% to 75% when the total flow rate is 5 m^3/h, for the water cut ranging from 50% to 60% when the total flow rate is 10 m^3/h. The completely stratified flow is identified by the X-ray tomography, which measures the vertical phase distribution of oil and water in the pipe.

4. Results and discussion

There are six simulations carried out in this study, as shown in Table 3. The flow patterns are oil-water stratified flow or oil single phase flow, and the developed model is available for prediction. Simulations 1 and 6 are carried out to verify the accuracy of the developed wax deposition model for the oil single-phase flow. Simulations 2 to 5 are carried out for oil-water stratified flow. Simulation 5 is used to predict wax deposit thickness circumferential distribution around the pipe wall.

4.1. Deposition results for single phase oil flow

The accuracy of the developed wax deposition model will be verified first for single phase flow, which the water cut is 0 in the experiment conducted by Hoffmann et al. (2012). The data from lab-scale experiment is the wax deposit weight per unit area based on the removable test section, at a fixed oil flow rate of 5 m^3/h and 10 m^3/h. This rather simple test sets the water property and flow rate to be the same as the oil. The oil-water interface is fictitious. As expected, the oil-water interface position is at the middle of the pipe and the interface shape is planner.

The amount of wax deposit formation and accumulation on the pipe wall is a critical variable of interest during wax deposit. The data from experimental wax deposition in lab-scale single phase oil flow is the weight and the wax content of layer deposit on the removable wax deposit test section. In order to expediently compare the results between experiment and prediction, the weight and the wax content of deposit layer $\overline{F}$ calculated by the model are given as

$$W_{\mathrm{dep}} = \pi D_{\mathrm{in,in}} \rho_{\mathrm{dep}} \int_{x=0}^{x=L_{\mathrm{r}}} \delta_x \mathrm{d}x = \pi D_{\mathrm{in,in}} \rho_{\mathrm{dep}} \sum_{i=0}^{i=M} (\delta_i h_i) \tag{27}$$

$$\overline{F} = \frac{\int_{x=0}^{x=L_{\mathrm{r}}} \overline{F}_x \delta_x \mathrm{d}x}{\int_{x=0}^{x=L_{\mathrm{r}}} \delta_x \mathrm{d}x} = \frac{\sum_{i=0}^{i=M} (\overline{F}_i \delta_i h_i)}{\sum_{i=0}^{i=M} (\delta_i h_i)} \tag{28}$$

Fig. 9 shows the comparison of the wax deposit weights measured at the end of the experiments, with the predictions by

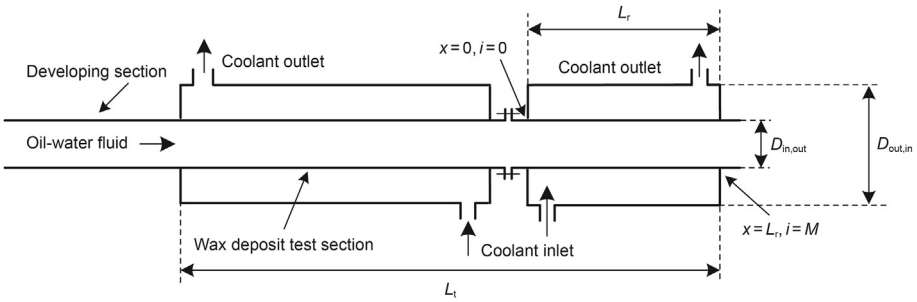

Fig. 7. Wax deposit test section.

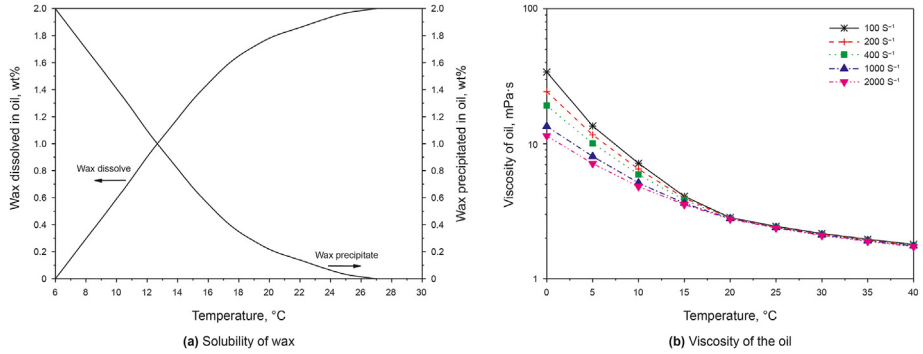

Fig. 8. Solubility of wax in the oil and viscosity of the oil.

Table 3
The operating conditions of experiment.

simulation number	total flow rate, m^3/h	water cut, %	oil flow rate, m^3/h	water flow rate, m^3/h	oil inlet temperature,°C	water inlet temperature,°C	duration, days
1	5.0	0	5.0	0	24.0	–	2
2	5.0	25.0	3.7	1.3	24.0	23.1	2.6
3	5.0	50.0	2.5	2.5	24.0	21.6	2.7
4	5.0	65.0	1.7	3.3	24.7	22.0	2.7
5	5.0	75.0	1.2	3.8	25.0	21.3	2.7
6	10	0	10.0	0	25	–	1.8

the model, for two different oil flow rates, i.e., Simulations 1 and 6 in Table 3.

It is observed that the present model gives well predictions of wax deposit weight per area compared with the experiments. The predictions are slightly higher than the experiments within 10% relative error, for both two oil flow rates, at the end of experiment 48 h and 43.2 h respectively. The predicted results show the deposit does not stop growing at the end of experiment, and it will continue to build up as the experiment lasted longer. The wax deposit decreases when oil flow rate increases from 5 m^3/s to 10 m^3/s. This is consistent with the previously reported single-phase wax deposit experiment of Hoffmann and Amundsen (2010), which performed by using the same oil and flow loop. The deposit rate is large in the initial stage, and then it gets smaller with enhanced thermal insulation of wax deposits caused by the increasing deposit thickness, and the mass driving force for further deposit decreases. Once the oil-deposit interface temperature reaches the WAT, the deposit will stop growing.

Fig. 10 gives the predicted wax content of the deposit for single phase flow with different oil flow rates. The wax content of the deposit for the oil flow rate of 10 m^3/h is higher than that for the oil flow rate of 5 m^3/h. The trend of the wax content of deposit with oil flow rate is in the opposite direction of the deposit thickness. At the same time, the wax content of the deposit does not stop increasing at the end of experiment. It will continue to increase with time, even though the deposit thickness stops growing. Although the oil-deposit interface temperature reaches the WAT, there is still a concentration gradient at the oil-deposit interface. This gradient causes mass driving force for an internal mass flux in deposit, which propel the wax content of the deposit to continue increasing with time.

The gelation can occur and form a deposit when the dynamic yield stress of the layer reaches ~3.5 Pa (Zheng et al., 2017), and exceeds the shear stress imposed by the fluid at the interface. The dynamic yield stress is positively correlated with the solid fraction of deposit layer. The shear stress at the wall is 1.35 Pa, for the oil flow rate of 5 m^3/h, and it is 4.54 Pa for the oil flow rate of 10 m^3/h, calculated by the above hydrodynamics model. The formed deposit must be with greater dynamic yield stress for higher oil flow rate. So an increase in the oil flow rate can lead to a decrease in the thickness of the deposit and an increase in the wax content of the deposit.

4.2. Deposition results for oil-water stratified flow

For oil-water stratified flow, wax deposition occurs only on the upper of pipe wall and the thickness distribution along the circumference is uneven. In order to compare the result between

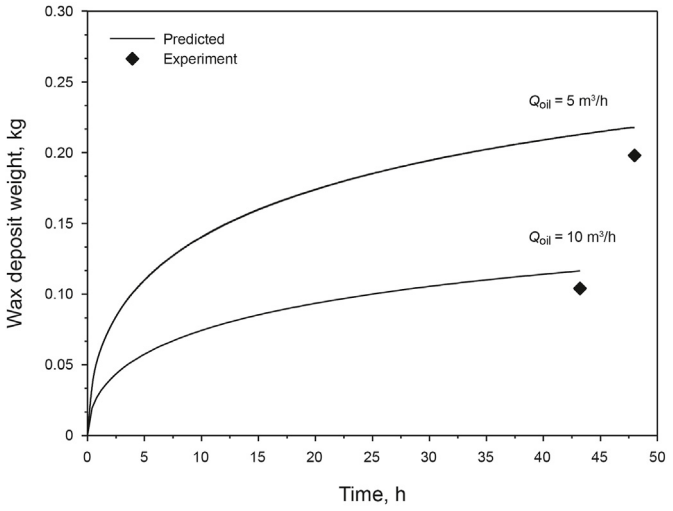

Fig. 9. Comparison between the experimental and the predicted deposit weight for single phase flow.

experiment and calculation expediently, the weight and the wax content of deposit layer on the removable test section calculated by the model are given as

$$W_{\mathrm{dep}} = \pi\rho_{\mathrm{dep}} \int_{x=0}^{x=L_{\mathrm{r}}} \int_{\eta=-7}^{\eta=-7} \delta_{x,\eta} l_\eta \mathrm{d}\eta \mathrm{d}x = \pi\rho_{\mathrm{dep}} \sum_{i=0}^{i=M} \sum_{k=0}^{k=P} (\delta_{i,k} h_i h_k l_\eta) \tag{29}$$

$$\overline{F} = \frac{\int_{x=0}^{x=L_{\mathrm{r}}} \int_{\eta=-7}^{\eta=-7} \overline{F}_{x,\eta} \delta_{x,\eta} l_\eta \mathrm{d}\eta \mathrm{d}x}{\int_{x=0}^{x=L_{\mathrm{r}}} \int_{\eta=-7}^{\eta=-7} \delta_{x,\eta} l_\eta \mathrm{d}\eta \mathrm{d}x} = \frac{\sum_{i=0}^{i=M} \sum_{k=0}^{k=P} (\overline{F}_{x,\eta} \delta_{i,k} h_i h_k l_\eta)}{\sum_{i=0}^{i=M} \sum_{k=0}^{k=P} (\delta_{x,\eta} h_i h_k l_\eta)} \tag{30}$$

In the experiment of Hoffmann et al. (2012), the completely oil-water stratified flow occurs for the water cut ranging from 30% to 80% when the total flow rate is 5 m^3/h, observed by the reflex camera pictures and the X-ray instrument. Therefore, the Simulations 2 to 5 are carried out to verify the accuracy of the developed

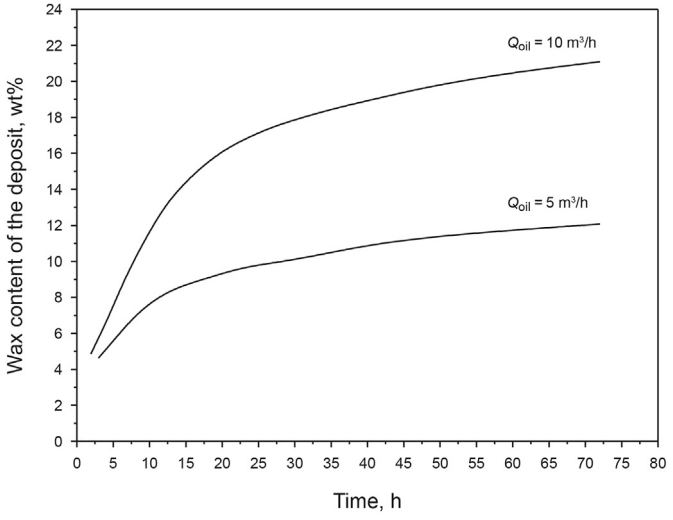

Fig. 10. The predicted wax content of the deposit for single phase flow.

wax deposition model for the oil-water stratified flow. The comparison of the weights of the wax deposit measured at the end of the experiments with the predictions of the model for different water cuts is shown in Fig. 11, where the total flow rate is 5 m^3/h and the duration of the experiment is 2.7 days. As can be seen, the predicted results of wax deposit weight are in good agreement with the experimental data. The simulation gives up-predictions within an average absolute error 15%. The average absolute relative error is 8.67%. The model gives the same variation trend of deposit weight with water cut as the experiment. That is the deposit weight first decreases and then increases as the water cut increased. It should be noted that the surface areas of the circular section in pipe covered by the wax deposit layer are different observed in experiments with different water cuts. The weight of wax deposit simultaneously related to the arc surface area covered by the deposit and the wax deposit rate under the same deposit duration condition.

Fig. 12 shows the comparison of arc surface area covered by the deposit divided by the internal surface area of the pipe with the predictions for different water cuts. It is noted that the oil-water interface configuration is definitely not planar and tends to curve. Meanwhile, the different values under curve oil-water interface and planar interface are compared to the experiment. The model assuming planar interface generally gives greatly under-prediction of surface area covered by the deposit. This underestimation becomes more severe as water cut increases. The model assuming curved interface mitigates the degree of underestimation. This mitigating is particularly pronounced in Simulation 5, i.e. the water cut 75%. Because the proportion of the wetted periphery by oil is 52.82% of the pipe inner circumference, obtained by the experimental camera pictures. However, the proportion is only 36.76% for the water cut 75%, if the interface configuration is planar. The proportion calculated by the model is 45.36%, which is 14.12% lower than the measured of 52.82%. It indicates that an accurate description of oil-water interface configuration is important when performing oil-water stratified two-phase flow calculations. The curved oil-water interface observed in some experiments (Edomwonyi-Otu and Angeli, 2015) and adopted in some numerical simulations (Pouraria et al., 2016; Liu et al., 2022). The model assuming curved interface gives under prediction of the arc surface area wetted by the oil is probably due to that the model doesn't take into account the increasing amount of water in the oil phase as the water cut increases from 50% to 80%. This can be observed by the water volume fraction distribution for at different water cuts in the experiment of Hoffmann et al. (2012).

Since the pipe inner wall surface area covered by the wax deposit varies with changing water cut, the amount of wax deposit accumulated on the pipe wall needs to be normalized with respect to the arc surface area covered by the deposit. The wax deposit rate is directly reflected by the weights of the deposit divided by the arc surface areas covered by the deposit, which is more reasonable and shown in Fig. 13. It can be seen that the weights per area of the deposit calculated by the model are higher than those for the deposition experiment, within an average absolute error 11.02%. Obviously, the deposit weights per area calculated by the present model are away from the experimental value with the water cut increasing. The deposit weight of experiment and prediction are 1.69 kg/m^2 and 1.78 kg/m^2, respectively, with 5.01% relative error, for 25% water cut; and for 50% water cut, the values are 1.64 kg/m^2 and 1.81 kg/m^2, with 9.87% relative error; and for 75% water cut, the values are 3.15 kg/m^2 and 3.66 kg/m^2, with 16.09% relative error. As shown in Figs. 11 and 13, the relative errors of the wax deposit weight and the weight per area obtained by the model have opposite trends with water cut increasing. The main reason for this difference is that the computation error of the arc surface areas

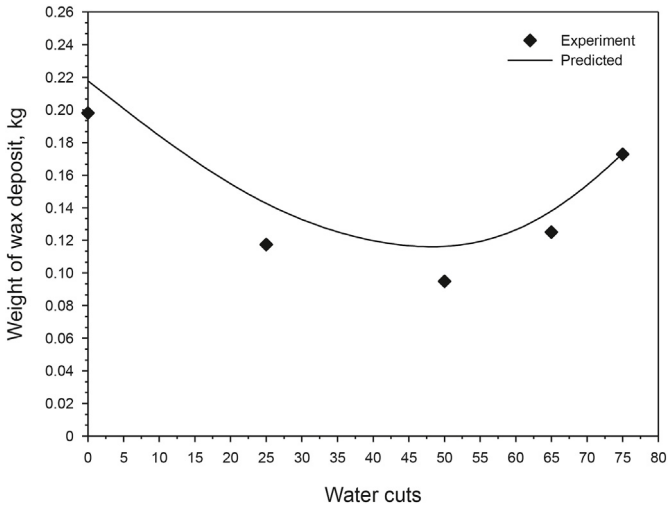

Fig. 11. Comparison of the experimental weights of the wax deposit with the predictions for different water cuts.

covered by the deposit, as shown in Fig. 12.

It is noted that the deposit weights per area at the water cuts of 65% and 75% are higher than those at the water cuts of 50%, for the wax deposit model and experiment in oil-water stratified flow. The weight of the deposit for water cut of 25% and total flow rate of 5 m^3/h is not listed, because the completely oil-water stratified flow occurs for the water cut ranging from 30% to 75% and total flow rate is 5 m^3/h in the experiment of Hoffmann et al. (2012). The mean wall shear stresses given by the hydrodynamics modeling for the water cuts of 50%, 65% and 75% conditions are 5.12 Pa, 4.36 Pa and 3.27 Pa for the oil domains, respectively. The wall shear stress (pressure gradient) decreases with the increase of water cut for oil-water stratified flow with constant oil-water total flow rate, which is confirmed by the experiments of Edomwonyi-Otu and Angeli (2015), and Liu et al. (2008). It can be seen from the wax gelation mechanism that an increase in water cut can help to reduce the wall/oil-deposit interface shear stress, thereby leading to an increase in the degree of gelation as well as the deposit rate. Furthermore, wax content of deposit layer for different water cuts predicted by the model is shown in Fig. 13. It indicates that an increase in water cut can lead to a decrease in the wax content of the deposit. The deposit formed at the higher water cut with lower wall/oil-deposit interface shear stress contains a significantly smaller amount of solid wax than the deposit formed at the lower water cut. This prediction is consistent with the experiment of Hoffmann et al. (2012) that the deposits with the water cuts of 65% and 75% have smaller fractions of the heavy components and their carbon number distributions of the wax deposit are more similar to the oil when compared to the deposit with water cut of 50%.

4.3. Deposit circumferential distribution for stratified flow

In the experiment of Hoffmann et al. (2012), the completely oil-water stratified flow occurs for the water cut ranging from 30% to 75% when the total flow rate is 5 m^3/h. As a result, the simulation 5 is used to predict wax deposit thickness circumferential distribution around the pipe wall. Fig. 14 shows the comparison of deposit thickness circumferential distribution at cross section of pipe calculated by the present model with the experiment measurement, for Simulation 5, i.e., the water cut 75%, the total flow rate 5 m^3/h. The results calculated by the model is in accordance with what was observed in the Hoffmann et al.'s (2012) experiment.

For water cut 75% and total flow rate 5 m^3/h, the model predicts the wax deposit weight of 0.173 kg, 1.33% higher than the measured of 0.172 kg at the end of the experiment. The deposit occurs only on the top of the pipe inner wall wetted by the oil for stratified flow, and the existence of water phase reduces the pipe wall area available for wax deposition. The wax deposit weight is influenced by the surface areas of the pipe covered by the deposit, and the pipe wall surface area covered by the wax deposit changes with variational water cut. Therefore, the deposit per unit surface area, i.e., the amount of wax attached to the pipe wall normalized with respect to the surface area covered by the deposit, is more reasonable variable of interest. The deposit per unit surface area calculated by the model is 3.656 kg/m^2, 16.08% higher than the experiment result of 3.149 kg/m^2. The surface areas covered by the deposit predicted by the model is 0.047 m^2, which is 14.1% lower than the measured of 0.055 m^2 obtained by the camera pictures of the wax deposit at the end of the experiment. In this case, the sector of wax deposit buildup predicted by the model is ranged from 0° to 81.5° and from 278.5° to 360°, and the measured is ranged from 0° to 106.8° and from 251.1° to 360°, where at the top of pipe, $a = 0°$, and at the bottom of pipe, $a = 180°$.

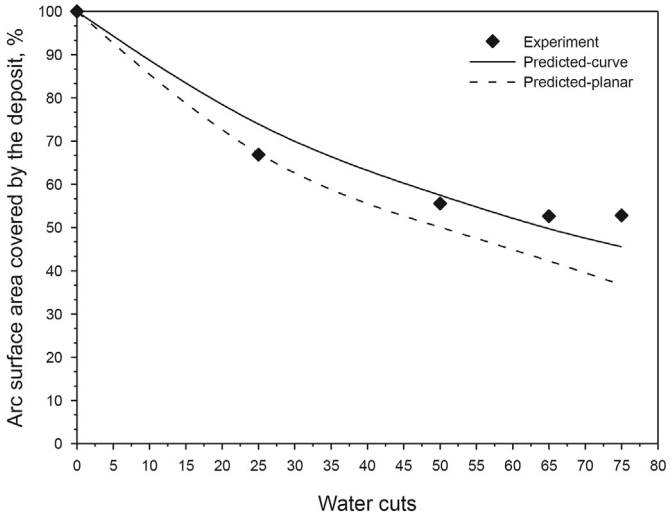

Fig. 12. Comparison of the arc surface area covered by the deposit with the predictions for different water cuts.

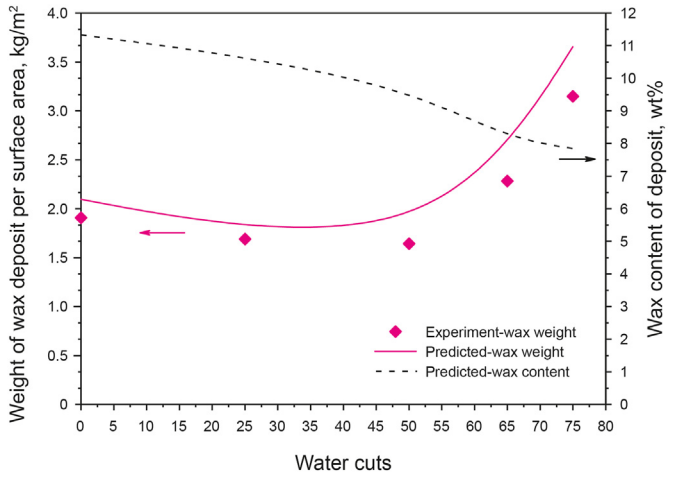

Fig. 13. Comparison of the experimental weights of the wax deposit per surface area of the pipe covered by the deposit with the predictions and the predicted wax content of the deposit layer for different water cuts.

The irregular shape of the deposit can be clearly determined from the camera picture at the end of experiment, which is no longer complete circular. Both the experiments and model predictions reveals that there is a plateau at the bottom of the pipe where the pipe inner wall wetted by the water and the wax thickness is zero. The experiment shows the wax deposition surface is uneven, and the thickness circumferential distribution is irregular. The thickest layer of wax deposits is 9.07 mm, located at the top of pipe. It is important to note that since the experimental thickness circumferential distribution obtained by the camera picture has a degree of uncertainties, the difference between the calculation and experiment could be a result of the impact of the camera picture. It can be clearly seen that the thickness circumferential distribution on pipe wall is roughly uniformly distributed locates near the top of the pipe, i.e. $\alpha = 0^\circ$. And the nearer the position gets close to two points, where the oil-water interface contacts the inner wall, the deposition thickness quickly drops to 0 from 10.35 mm, calculated by the model.

It is attributed to the fact that a roughly uniformly thickness far away from the oil-water interface contact the inner wall results in the slowly changes temperature along the circumferential pipe wall wetted by oil, from 16.9 °C to 16.5 °C with α vary from 0° to 81.5°, resulting in an almost constant mass flux from the bulk oil to the oil-deposit interface, leading to a slowly varying of the deposit layer thickness. The circumferential temperature distribution at pipe wall is consistent with the numerical simulation of Li et al. (2018).

The deposit thickness circumferential distribution at pipe wall for stratified oil-water flow is different from the stratified oil-gas flow, although the wax deposit only occurs on the wall contacting with oil for these two stratified flows. The deposit is distributed in a crescent shape with two identifiable zones, which is observed in the experiment of Matzain et al. (2002), Gong et al. (2011) and Chi et al. (2019), and simulated by Duan et al. (2016, 2017). The wax deposit thickness is not uniformly distributed along the circumference not just at the oil-gas interface contact wall but also at the bottom of the pipe, where the deposit thickness reaches its maximum. The reason, Duan et al. (2016, 2017) pointed out, is mainly that the non-uniform circumferential distributions of the wax mass flux at oil-deposit interface and the solubility gradient of oil at the oil-deposit interface, which is resulted from the non-uniform temperature circumferential distribution at oil-deposit interface. Therefore, the wax thickness circumferential distribution near the top of the pipe is roughly uniformly, which is attributed to the slowly change of temperature along the circumferential oil-deposit interface. The temperature circumferential distribution at pipe wall of oil phase and far away from the immiscibility phase interface contact the inner wall for stratified oil-water flow is different from the stratified oil-gas flow. This is due to the specific heat capacity and heat conductivity of the gas phase is smaller than water phase.

Fig. 14b shows the wax content of deposit layer circumferential distribution at cross section of pipe calculated by the present model, for Simulation 5, i.e., the water cut 75%, the total flow rate 5 m^3/h. The wax content of the deposit is closely related to the hardness of the deposit, which is significant for wax removing in pipe, in terms of cleaning method designing and pigging operation.

The maximum wax content of deposit, 9.76%, locates at the top of the pipe, and the minimum, 7.02%, locates at the oil-water interface contact wall. It is very similar to the experiment of Anosike (2007). The wax content distribution of deposit layer is nearly constant, except close to the oil-water interface where they decrease dramatically. It may be attributed to the fact that a higher oil-deposit interface shear stress at the top of the pipe, leading to a greater dynamic yield stress of deposit layer with higher wax content of the formed deposit. The interface shear stress in oil phase is nearly constant near the top of the pipe, and decreases toward the oil-water interface, from 5.43 Pa to 2.95 Pa.

5. Conclusion

The stratified oil-water two-phase flow often presents in horizontal or slightly onshore and offshore oil production pipe systems, and is considered to be among the fundamental flow configuration in two-phase systems. Wax deposition in oil-water stratified flow is a common occurrence and typically reduces transportation capacity of oil. Accurate prediction of wax deposition is of great importance to develop economical prevention and remediation strategies. However, a reliable mechanistic model for wax deposition prediction in oil-water two-phase stratified pipe flow is lacking to validate the deposition process.

In this work, a three-dimensional (axial, radial, and angular) robust wax deposit model for oil-water stratified circular pipe flow was developed. The model of formation of a gel deposit based on the first principles of rheology was developed, associated with the results obtained from hydrodynamics and heat/mass transfer simulations. Due to the non-circular and irregular oil and water domains in stratified pipe flow, computations were performed in the bipolar coordinate system for convenient mapping of the physical domain.

The six simulation results of wax deposit were compared with the experimental measurements with a flow loop. The predicted deposit thickness of single phase for oil flow rate of 5 m^3/h and

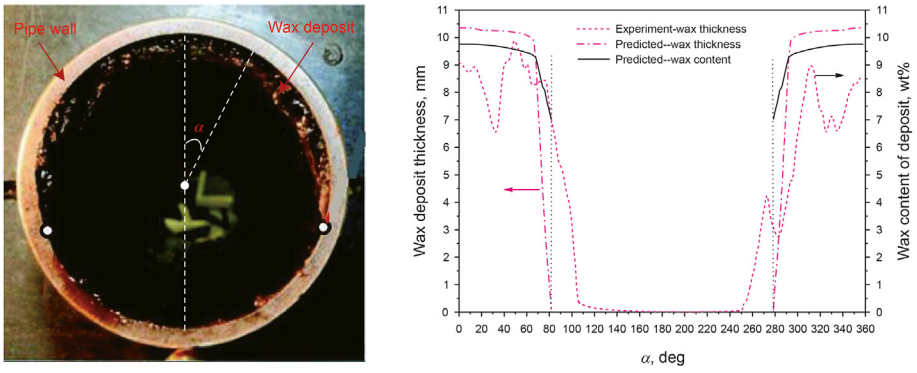

(a) Camera picture (Hoffmann et al., 2012)

(b) Deposit thickness and wax content of the deposit circumferential distribution

Fig. 14. The comparison of deposit thickness circumferential distribution at cross section of pipe.

10 m^3/h were reasonably agreed with experimental data. The predictions were slightly higher than the experiments within 10% relative error, for both two oil flow rates, at the end of experiment 48 h and 43.2 h respectively. And the model gave the predicted wax content of the deposit for single phase flow with different oil flow rates. It indicated that an increase in the oil flow rate can lead to a decrease in the thickness of the deposit and an increase in the wax content of the deposit.

For oil-water stratified flow, the deposition only occurs at and above the oil-water interface. The predictions for the wax deposit weight per surface area of the pipe covered by the deposit were found to compare satisfactorily with experimental data with four different water cut 25%, 50.0%, 65.0%, 75.0%, for oil-water stratified pipe flow. It can be seen from the wax gelation mechanism that an increase in water cut can help to reduce the wall/oil-deposit interface shear stress, thereby leading to an increase in the degree of gelation as well as the deposit rate.

A local deposit analysis in the circumferential direction was conducted, for water cut 75% and total flow rate 5 m^3/h, which provided insights to understand that the thickness on pipe wall was roughly uniformly distributed locates near the top of the pipe and the nearer the position gets close to two points, where the oil-water interface contacts the inner wall, the deposition thickness quickly dropped to 0. It was attributed to the fact that a roughly uniformly thickness far away from the oil-water interface contact the inner wall resulted in the slowly changes temperature along the circumferential pipe wall wetted by oil. Furthermore, the deposit thickness circumferential distribution at pipe wall for stratified oil-water flow was different from the stratified oil-gas flow This was due to the specific heat capacity and heat conductivity of the gas phase is smaller than water phase.

Acknowledgments

The work received the support of by National Natural Science Foundation of China (52272338), Major Project of Science and Technology Research Program of Chongqing Education Commission of China (KJZD-M202212901, KJZD-K202012903), Young Elite Scientists Sponsorship Program (2020-JCJQ-QT-005).

Notation

Variables

A	cross-sectional area inside the pipe, m^2
C	wax concentration in crude oil, kg/m^3
D	diameter of the pipe, m
$D_{in,in}$	inner diameter of inner pipe, m
$D_{in,out}$	out diameter of inner pipe, m
D_{eff}	effective diffusivity in the deposit, m^2/s
dP/dz	pressure gradient, Pa/m
D_{WO}	diffusivity wax in crude oil, m^2/s
Eo	Eötvös number
F_w	wax fraction in the deposit, wt%
$\overline{F}_w$	average wax fraction in the deposit, wt%
G	mass flow rate, kg/s
K	consistency of fluid, $Pa \cdot s^n$
a	half distance between the two polar points, m
g	gravitation, m/s^2
H_W	water cut
h_e	overall heat transfer coefficient, $W/(m^2 \cdot K)$
h_W	water level for plane interface,m
h_0	heat transfer coefficient, $W/(m^2 \cdot K)$
i, j, k	coordinate of mesh point at x ξ, η, coordinate direction
$J_{A,\xi}, J_{A,\eta}, J_{B,\xi} J_{B,\eta}$	mass flux of wax molecules into the deposit, $kg\ m^{-1}\ s^{-1}$
J_{wax}	mass flux of wax molecules from the oil to oil-deposit interface, $kg\ m^{-1}\ s^{-1}$
L	length of pipe, m
l_ξ, l_η, l_x	scale factors of bipolar coordinate system
M_{tot}	the total deposited wax mass, kg
n	flow index of oil
Pr	Prandtl number
Q	flow rate, m^3/s
R	radius of pipe, m
S_φ	generalized source term
Sc	Schmidt number
T	temperature, °C
T_∞	ambient temperature, °C
t	time, s
V_{tot}	total volume in the closed system, m^3
u	velocity in the axial direction, m/s
x, y, z	axial coordinate in Cartesian system, m

Greek Leteers

α	equivalent crystal aspect ratio
$\tilde{\alpha}$	solid-fluids wettability angle
τ	shear stress, Pa
Γ_T	effective thermal diffusivity
Γ_w	effective viscosity, m^2/s
Γ_C	effective mass transfer
Γ_φ	generalized diffusivity
$\dot{\gamma}$	strain rate magnitude, s^{-1}
γ	circumferential angle, °
$\Delta\rho$	density difference between oil and water, kg/m^3
δ	deposit thickness, m
θ^*	oil-water interface, rad
θ_0^P	oil distribution angle for plane interface configuration, rad
θ_1	upper section of the pipe wall, rad
θ_2	the angle for interface, rad
φ	porosity of the deposit layer
λ	heat conductivity coefficient, $W/(m \cdot K)$
μ_m	kinematic viscosity coefficient, m^2/s
μ_t	eddy diffusivity for momentum, m^2/s
x, ξ, η	coordinate in bipolar system
ρ	density, kg/m^3
σ	interfacial tension between oil and water,N/m
Θ	wetted wall fraction

Subscripts

O	properties of the oil
I	properties of the oil-water interface
W	properties of the water
bulk	properties at the bulk
dep	properties of the deposit
envir	properties of the coolant liquid
i, j, k	coordinate of mesh point at ξ, η, z coordinate direction
in	properties at the inlet
wax	properties of the wax

References

Anosike, C.F., 2007. Effect of Flow Patterns on Oil-Water Flow Paraffin Deposition in Horizontal Pipes. PhD Dissertation. The University of Tulsa.

Bai, J., Jin, X., Wu, J., 2019. Multifunctional anti-wax coatings for paraffin control in oil pipelines. Petrol. Sci. 16, 619–631. https://doi.org/10.1007/s12182-019-0309-7.

Bordalo, S.N., Oliveira, R.D., 2007. Experimental Study of Oil/Water Flow with Paraffin Precipitation in Submarine Pipelines. SPE Annual Technical Conference

and Exhibition, p. 8. Society of Petroleum Engineers, Anaheim, California, U.S.A.
Brauner, N., Rovinsky, J., Moalem Maron, D., 1996. Determination of the interface curvature in stratified two-phase systems by energy considerations. Int. J. Multiphas. Flow 22, 1167–1185. https://doi.org/10.1016/0301-9322(96)00046-8.
Chakrabarti, D.P., Das, G., Ray, S., 2005. In: Pressure Drop in Liquid-Liquid Two Phase Horizontal Flow: Experiment and Prediction, vol. 28, pp. 1003–1009.
Chi, Y., Sarica, C., Daraboina, N., 2019. Experimental investigation of two-phase gas-oil stratified flow wax deposition in pipeline. Fuel 247, 113–125. https://doi.org/10.1016/j.fuel.2019.03.032.
Chilton, R.A., Stainsby, R., 1998. Pressure loss equations for laminar and turbulent non-Newtonian pipe flow. J. Hydraul. Eng. 124, 522–529. https://doi.org/10.1061/(ASCE)0733-9429(1998)124:5(522).
Cussler EL, H.S.W.W., 1988. Barrier Membranes, pp. 161–174.
Duan, J., Liu, H., Guan, J., Hua, W., Jiao, G., Gong, J., 2016. Wax deposition modeling of oil/gas stratified smooth pipe flow. AIChE J. 62, 2550–2562. https://doi.org/10.1002/aic.15223.
Duan, J., Liu, H., Jiang, J., Xue, S., Wu, J., Gong, J., 2017. Numerical prediction of wax deposition in oil–gas stratified pipe flow. Int. J. Heat Mass Tran. 105, 279–289. https://doi.org/10.1016/j.ijheatmasstransfer.2016.09.082.
Edomwonyi-Otu, L.C., Angeli, P., 2015. Pressure drop and holdup predictions in horizontal oil–water flows for curved and wavy interfaces. Chem. Eng. Res. Des. 93, 55–65. https://doi.org/10.1016/j.cherd.2014.06.009.
Gong, J., Zhang, Y., Liao, L., Duan, J., Wang, P., Zhou, J., 2011. Wax deposition in the oil/gas two-phase flow for a horizontal pipe. Energy Fuel. 25, 1624–1632. https://doi.org/10.1021/ef101682u.
Gorelik, D., Neima, B., 1999. The interface configuration in two-phase stratified pipe flows. Int. J. Multiphas. Flow 25, 977–1007. https://doi.org/10.1016/S0301-9322(99)00038-5.
Hayduk W, M.B., 1982. Correlations for Prediction of Molecular Diffusivities in Liquids, pp. 295–299.
Hoffmann, R., Amundsen, L., 2010. Single-phase wax deposition experiments. Energy Fuel. 24, 1069–1080. https://doi.org/10.1021/ef900920x.
Hoffmann, R., Amundsen, L., Huang, Z., Zheng, S., Fogler, H.S., 2012. Wax deposition in stratified oil/water flow. Energy Fuel. 26, 3416–3423. https://doi.org/10.1021/ef2018989.
Huang, Z., Lee, H.S., Senra, M., Scott Fogler, H., 2011a. A fundamental model of wax deposition in subsea oil pipelines. AIChE J. 57, 2955–2964. https://doi.org/10.1002/aic.12517.
Huang, Z., Senra, M., Kapoor, R., Fogler, H.S., 2011b. Wax deposition modeling of oil/water stratified channel flow. AIChE J. 57, 841–851. https://doi.org/10.1002/aic.12307.
Janamatti, A., Lu, Y., Ravichandran, S., Sarica, C., Daraboina, N., 2019. Influence of operating temperatures on long-duration wax deposition in flow lines. J. Petrol. Sci. Eng. 183, 106373. https://doi.org/10.1016/j.petrol.2019.106373.
Kays William, M., 1994. Turbulent Prandtl number—where are we? Asme Transac. J. Heat Trans. 116, 284–295.
Li, Y., He, G., Sun, L., Ding, D., Liang, Y., 2018. Numerical simulation of oil-water non-Newtonian two-phase stratified wavy pipe flow coupled with heat transfer. Appl. Therm. Eng. 140, 266–286. https://doi.org/10.1016/j.applthermaleng.2018.05.048.
Liu, H., Duan, J., Li, J., Gu, K., Lin, K., Wang, J., Yan, H., Guan, L., Li, C., 2022. Numerical quasi-three dimensional modeling of stratified oil-water flow in horizontal circular pipe. Ocean Eng. 251, 111172. https://doi.org/10.1016/j.oceaneng.2022.111172.
Liu, Y., Zhang, H., Wang, S., Wang, J., 2008. Prediction of pressure gradient and holdup in small Eötvös number liquid-liquid segregated flow. Chin. J. Chem. Eng. 16, 184–191. https://doi.org/10.1016/S1004-9541(08)60060-9.
Liu, Z., Li, Y., Wang, W., Song, G., Lu, Z., Ning, Y., 2020. Wax and wax–hydrate deposition characteristics in single-, two-, and three-phase pipelines: a review. Energy Fuel. 34, 13350–13368. https://doi.org/10.1021/acs.energyfuels.0c02749.
Mahir, L.H.A., 2020. Modeling Paraffin Wax Deposition from Flowing Oil onto Cold Surfaces. PhD Dissertation. University of Michigan.
Mahir, L.H.A., Lee, J., Fogler, H.S., Larson, R.G., 2021. An experimentally validated heat and mass transfer model for wax deposition from flowing oil onto a cold surface. AIChE J. 67. https://doi.org/10.1002/aic.17063.
Mahir, L.H.A., Vilas Bôas Fávero, C., Ketjuntiwa, T., Fogler, H.S., Larson, R.G., 2019. Mechanism of wax deposition on cold surfaces: gelation and deposit aging. Energy Fuel. 33, 3776–3786. https://doi.org/10.1021/acs.energyfuels.8b03139.
Matzain, A., Apte, M.S., Zhang, H., Volk, M., Brill, J.P., Creek, J.L., 2002. Investigation of paraffin deposition during multiphase flow in pipelines and wellbores—Part 1: experiments. J. Energy Resour. Technol. 124, 180. https://doi.org/10.1115/1.1484392.
Ng, T.S., Lawrence, C.J., Hewitt, G.F., 2001. Interface shapes for two-phase laminar stratified flow in a circular pipe. Int. J. Multiphas. Flow 27, 1301–1311. https://doi.org/10.1016/S0301-9322(01)00005-2.
Piroozian, A., Hemmati, M., Ismail, I., Manan, M.A., Rashidi, M.M., Mohsin, R., 2017. An experimental study of flow patterns pertinent to waxy crude oil-water two-phase flows. Chem. Eng. Sci. 164, 313–332. https://doi.org/10.1016/j.ces.2017.02.026.
Pouraria, H., Seo, J.K., Paik, J.K., 2016. Numerical modelling of two-phase oil–water flow patterns in a subsea pipeline. Ocean Eng. 115, 135–148. https://doi.org/10.1016/j.oceaneng.2016.02.007.
Quan, Q., Wang, W., Wang, P., Duan, J., Yang, J., Yao, H., Gong, J., 2015. Wax deposition from emulsion-water in stratified flow. Petrol. Sci. Technol. 33, 749–755. https://doi.org/10.1080/10916466.2015.1007381.
Santos, D.S., Faia, P.M., Garcia, F.A.P., Rasteiro, M.G., 2019. Oil/water stratified flow in a horizontal pipe: simulated and experimental studies using EIT. J. Petrol. Sci. Eng. 174, 1179–1193. https://doi.org/10.1016/j.petrol.2018.12.002.
Singh, P., Venkatesan, R., Fogler, H.S., Nagarajan, N., 2000. Formation and aging of incipient thin film wax-oil gels. AIChE J. 46, 1059–1074. https://doi.org/10.1002/aic.690460517.
Van Der Geest, C., Guersoni, V.C.B., Merino-Garcia, D., Bannwart, A.C., 2018. Wax deposition experiment with highly paraffinic crude oil in laminar single-phase flow unpredictable by molecular diffusion mechanism. Energy Fuel. 32, 3406–3419. https://doi.org/10.1021/acs.energyfuels.8b00269.
Van der Geest, C., Melchuna, A., Bizarre, L., Bannwart, A.C., Guersoni, V.C.B., 2021. Critical review on wax deposition in single-phase flow. Fuel 293, 120358. https://doi.org/10.1016/j.fuel.2021.120358.
Yang, J., Lu, Y., Daraboina, N., Sarica, C., 2020. Wax deposition mechanisms: is the current description sufficient? Fuel 275, 117937. https://doi.org/10.1016/j.fuel.2020.117937.
Zhang, X., Huang, Q., Zhang, Y., Gao, X., Chen, W., 2022. Predicting the yield stress of oil-wax gels with long-chained n-alkanes. J. Petrol. Sci. Eng. 208, 109238. https://doi.org/10.1016/j.petrol.2021.109238.
Zheng, S., Saidoun, M., Palermo, T., Mateen, K., Fogler, H.S., 2017. Wax deposition modeling with considerations of non-Newtonian characteristics: application on field-scale pipeline. Energy Fuel. 31, 5011–5023. https://doi.org/10.1021/acs.energyfuels.7b00504.